Published in final edited form as:
Combust Flame. 2020 May ; 215: 389–400. doi:10.1016/j.combustflame.2020.02.004.

The gas-phase formation of tin dioxide nanoparticles in single droplet combustion and flame spray pyrolysis

Haipeng Li[a,b], **Suman Pokhrel**[a,b], **Marco Schowalter**[c], **Andreas Rosenauer**[c], **Johannes Kiefer**[a,d], **Lutz Mädler**[a,b,*]

[a]Faculty of Production Engineering, University of Bremen, Badgasteiner Straße 1, 28359 Bremen, Germany

[b]Leibniz Institute for Materials Engineering IWT, Badgasteiner Straße 3, 28359 Bremen, Germany

[c]Institute of Solid State Physics, Electron Microscopy, University of Bremen, 28359 Bremen, Germany

[d]Technische Thermodynamik, University of Bremen, Badgasteiner Straße 1, 28359 Bremen, Germany

Abstract

Tin dioxide (SnO_2) nanoparticles synthesized *via* flame spray pyrolysis (FSP) have promising applications for gas sensors. The formation of SnO_2 nanoparticles in the gas-phase has been investigated using single droplet combustion and FSP. Precursor solutions of Tin (II) 2-ethylhexanoate dissolved in Xylene with varying Sn concentrations were selected as the precursor-solvent system. The selected precursor-solvent system has its stability and ability to synthesize homogeneous nanoparticles, compared to metal nitrate based precursor solutions. The precursor-solvent system was studied using attenuated total reflection Fourier transform infrared (ATR-FTIR) spectroscopy and thermogravimetric analysis (TGA). The SnO_2 nanoparticles were characterized using X-ray diffraction (XRD), Brunauer–Emmett–Teller (BET), and transmission electron microscopy (TEM). Droplet surface micro-explosions were observed during the single droplet combustion of the precursor solutions. It is because of the heterogeneous vapor-phase nucleation, which is beneath the liquid droplet surface and caused by precursor thermal decomposition. The results show that the size of nanoparticles obtained both from FSP and single droplet combustion increases with increasing metal-precursor concentration. The TEM images of the particles from such droplet combustion reveal two types of nanoparticles with different sizes and morphologies. The current work provides fundamental understanding of precursor decomposition and particle formation during single droplet combustion, which help in-depth understanding of the flame spray pyrolysis.

*Corresponding author at: Faculty of Production Engineering, University of Bremen, Leibniz Institute for Materials Engineering IWT, Badgasteiner Straße 3, 28359, Bremen, Germany. lmaedler@iwt.uni-bremen.de (L. Mädler).

Declaration of Competing Interest
None.

Europe PMC Funders Author Manuscripts

Keywords

SnO_2 nanoparticles; Flame spray pyrolysis; Single droplet combustion; Droplet surface micro-explosion; Nanoparticle comparison

1 Introduction

Flame spray pyrolysis (FSP) is a versatile technique for the fast and scalable synthesis of a wide variety of single- and multi-component metal oxide nanoparticles [1]. Almost every metal element in the periodic table can be utilized [1, 2]. High temperature pyrolysis, large thermal gradient, and fast quenching rate owing to the high-velocity spray flame result in a one-step process for synthesizing ultrafine nanoparticles with high purity [3]. The FSP technique is very appealing because of the possibility of controlling the particle size, the crystallinity, and the straight forward scale-up [3, 4]. Recently, the exploration of low-volatility and low-cost precursors [5, 6], nanoscale mixing using double-flame spray [7], and the functional applications in sensors, catalysis, phosphors, electroceramics, membranes, super-hydrophilic coatings, batteries, electrode fabrication, nanoparticle film fabrication, and biomaterials [1, 2, 8], made it even more attractive.

There are two known particle formation routes in the FSP process. One is gas-to-particle conversion. The entire vaporization of the precursor into the flame, followed by subsequent conversion in the gas phase, leads to homogeneous particle formation [5, 6, 9]. The other is droplet-to-particle conversion. Incomplete vaporization of the precursor causing precipitation and conversion within the spray droplets results in large, dense or hollow nanoparticles [5, 10, 11]. Even the latter route is suitable for the synthesis of ceramic powders and films [10]. However, most of the current and past research studies focus on promoting the former route to obtain homogeneous particles due to their wider applicability [12, 13]. To attain this target, a fundamental understanding of the droplet evaporation and combustion processes is necessary as they influence the precursor decomposition and particle nucleation. However, experimental investigations on the spray flame are challenging because of the interaction of droplets, the high flame temperature, the steep temperature gradients, the turbulence caused by the dispersion, and the short time scales. As an alternative, single droplet combustion has been used to understand (1) the formation from droplet to particle, (2) the comparison of nanoparticles obtained from single droplet combustion and from FSP, and (3) the exploration of low-volatility and low-cost precursors [14, 15]. Rosebrock et al. [16] investigated single droplet combustion with the precursor solutions used for FSP, and observed the disruptive combustion (also known as micro-explosion). Li *et al.* [17] employed a highly reactive precursor in single droplet combustion and observed similar phenomena. In order to study the influence of droplet micro-explosion on nanoparticle formation, single droplet combustion experiments of economic and low volatile precursors were conducted by Rose-brock *et al.* [14]. They found that adjusting the solvent can induce micro-explosion of droplets containing low volatile precursors. The comparison of particles synthesized from FSP with those from single droplet combustion showed that droplet micro-explosions contribute to yield homogeneous nanoparticles even using low volatile nitrate precursors. Meierhofer *et al.* [15] applied single droplet

combustion to interpret the phase impurities and multi-modal particle diameters caused by unwanted droplet-to-particle conversion routes during screening various precursor solutions for $Li_4Ti_5O_{12}$ energy storage materials. Residuals induced by flame extinction and incomplete vaporization of the precursors were observed during single droplet combustion. This was identified as a reason for the formation of inhomogeneous particles. However, using 2-ethylhexanoate acid (2-EHA) instead of ethanol as the solvent could reduce the occurrences of residuals and improve the complete vaporization, leading to homogenous particles. They also found the particles obtained from single droplet combustion and FSP were similar in size, crystalline state and phase purity. This further corroborates the hypothesis that single droplet combustion enables the prediction of the product quality, interpret the cause of particle formation, and seek solutions to improve the production of homogeneous nanoparticles in FSP. Moreover, the experimental data from single droplet combustion has been recently used in the simulation of particle synthesis by FSP [18]. In spite of these promising findings, related investigations are still lacking, and hence the detailed knowledge is yet to be acquired. The target of the present work is to fill this gap with an in-depth investigation in the role of droplet micro-explosions in the synthesis of homogeneous particles during single droplet combustion, and extend the research work to predict particle formation in FSP.

Here, we present the experimental investigation on tin dioxide (SnO_2) nanoparticles using Tin (II) 2-ethylhexanoate diluted with Xylene as the precursor-solvent system. This precursor-solvent system has proven to be able to synthesize homogeneous SnO_2 nanoparticles and promising SnO_2 -based sensors [19–21]. The optical measurements, interferometric particle imaging (IPI) and standard rainbow refractometry (SRR), have been carried out on single droplet combustion of this precursor-solvent system. The mass and heat transfer inside the burning droplets were estimated based on a multicomponent diffusion limited model [22]. Further investigation on nanoparticle formation from single droplet combustion is a key to provide fundamental understanding of the liquid-vapor-flame-particle process chain, which is a prerequisite for widening and designing the industrial applications of FSP for more complex nanomaterials [23]. In this work, we used the same precursor-solvent system with varying molarities of Sn to synthesize SnO_2 nanoparticles *via* both single droplet combustion and FSP. In order to develop a detailed understanding of the mechanisms, the initial stability and vaporization behavior of the precursor solutions was studied using Fourier-transform infrared (FTIR) spectroscopy and thermogravimetric analysis (TGA), respectively. The nanoparticles obtained from FSP were characterized by X-ray diffraction (XRD) and Brunauer–Emmett–Teller (BET) measurements. The morphologies and size distributions were compared to nanoparticles from single droplet combustion and FSP using transmission electron microscopy (TEM). 2.

2 Experimental setup and procedure

2.1 Single droplet combustion

Experiments on single droplet combustion were conducted under the conditions of normal gravity, normal pressure and room temperature. Figure 1 shows the sketch of the experimental setup. The droplet-on-demand generator (Piezodropper [24, 25]) was used to

obtain single isolated droplets at a frequency of 4 Hz. The droplets were ignited by the spark created by two electrodes in the co-flowing dry oxygen (purity 99.95%). The burning droplets ejected upwards in a square glass cuvette. The combustion processes were recorded *in-situ* with a high-speed camera (Fastcam SA4) at a frame rate of 40,000 Hz and a spatial resolution of 64 lp/mm (determined using a 1951 USAF resolution test target, Thorlabs, R1DS1P). The camera chip has 1024 ×96 pixels (L ×W) with a pixel size of 6.25 ×6.25 μm^2, which yields a field of view of 6.4 ×0.6 mm^2 (LxW). The recorded image has a pixel resolution of 37.80 pixels/cm. The shutter time of the high-speed camera is 1/178,000 s. Adjustments were conducted first during experiments in order to obtain stable droplets and flames, whose trajectories slightly vary and were recoded in-focus using the high-speed camera. The depth of focus of the high-speed camera is ±4.5 μm, and thus the variations of the droplet trajectory in the depth position is below 9 μm. The merged images of droplets presented in this work were cropped in the length direction to remove unnecessary parts. Resulting nanoparticles from the single droplet combustion were deposited on carbon-coated copper grids (Plano GmbH-S162), which were placed directly above the burning droplets at a distance of 10 mm. The collection time was 30 min. More details on setup and the experimental process of single droplet combustion can be found in Refs. [16, 17].

2.2 Flame spray pyrolysis

The nanoparticle synthesis using FSP was performed with a two-fluid nozzle as described by Mädler et al. [3]. The precursor solutions were mixed for 5 min with an ultrasonic vibrator, and then supplied to the nozzle with a 100 mL syringe pump at a flow rate of 5 mL/min. The dispersed oxygen with a flow rate of 5 L/min at a pressure of 1.5 bar was used to atomize the solution into small droplets. A concentric supporting flamelet ring of pre-mixed methane/oxygen (flow rate: methane 1.5 L/min and oxygen 3.2 L/min) was implemented to ignite the atomized droplets in order to maintain the spray flame. In FSP, a glass microfiber filter (GF/D Whatman, 257 mm in diameter) was installed in a water-cooled holder, which is fixed at a distance of 600 mm downstream of the nozzle. A vacuum pump was utilized to create gas flow through the glass fiber filter, promoting the deposition of particles on the filter during flame spray. The nanoparticles are removed by shave. Detailed descriptions of FSP setup and the experimental process can be found in Refs. [3].

2.3 Precursor solution preparation and analysis

Tin (II) 2-ethylhexanoate (Sigma-Aldrich, 93.3% purity, abbreviated as Tin 2-EHA here) was diluted with Xylene (VWR, 98.5% purity) to prepare precursor solutions with Sn molar concentrations of 0.05, 0.1, 0.25, 0.5, 0.75 and 1 mol/L. These six solutions were used for both single droplet combustion and FSP experiments.

The FTIR spectra of the prepared solutions were acquired in the wavenumber range from 650 to 4000 cm^{-1} with a nominal resolution of 2 cm^{-1} using an Agilent Cary 630 instrument equipped with a ZnSe unit for attenuated total reflection (ATR, five reflections at 45°). A high signal-to-noise ratio of each sample was obtained by averaging 32 scans. The measurements were performed at room temperature. A small glass cap was used to cover the sample on the ATR crystal, in order to avoid sample evaporation.

The vaporization behavior of the investigated precursor solutions was assessed with thermogravimetric analysis and differential thermal analysis (TGA-DTA, Netzsch STA 449 Jupiter). The liquid solutions (mass: ~50 mg) were placed in Al_2O_3 crucibles (Waters GmbH, 864305.003, OD = 6 mm, Height = 7.5 mm). The measurements were conducted under a flow of 50 mL/min synthetic air from 30 to 600 °C at an increased temperature rate of 7.5 °C/min.

2.4 Particle characterizations

Brunauer–Emmett–Teller (BET) measurements were performed using the Quantachrome NOVA 40 0 0e gas sorption system, in order to determine the specific surface area (SSA) and the average equivalent primary particle size (BET particle diameter) of the FSP-synthesized nanoparticles. The particles (mass: ~100 mg) were weighed and placed in test cells, and then pre-heated with de-gassing for 2 h at 200 °C in the flowing nitrogen atmosphere in order to clean the particle surface. During the BET measurements, liquid nitrogen was adopted as the adsorbent at 77 K. The BET diameter d_{BET} is calculated using the following equation:

$$d_{BET} = 6/SSA_{\rho_p}$$

where ρ_p is the density of SnO_2 (6.85 g/cm 3).

X-ray diffraction (XRD) measurements were performed using a PANalytical X'Pert MPD Pro-system with Ni-filtered $CuK_{\alpha 1\text{-}\alpha 2}$ radiation. The diffraction patterns were recorded by a PANalytical X'Celerator detector with 127 channels in the continuous scanning mode in the 2θ range from 20 °to 80 °with a step size of 0.016° and a measurement time step of 200 s. A fixed divergence of 1/4° was applied together with primary and secondary Soller slits of 0.04 and 0.0175 rad, in order to reduce the effects of over irradiation and asymmetry, respectively.

Carbon-coated copper grids (Plano GmbH-S162) were used as nanoparticle support for the single droplet combustion and FSP synthesized particles. Low- and high-resolution transmission electron microscopy (HRTEM) images were recorded using a Titan 80–300 ST microscope (FEI™) equipped with a Cs corrector for the imaging lens using a 300 keV electron beam. 3.

3 Results and discussion

This section presents the results in a systematic manner: (1) The analysis of the precursor solutions to understand their stability. (2) The results from single droplet combustion and FSP experiments. (3) The analysis of the synthesized nanoparticles from single droplet combustion and FSP. (4) The proposed mechanism of nanoparticle formation.

3.1 Analysis of precursor solutions

Infrared spectroscopy is an ideal technique for analyzing the stability of the precursor solutions as it is not only sensitive to the breakage and formation of covalent bonds, but also

allows extracting information about molecular interactions such as hydrogen bonding. Figure 2a and b shows the FTIR spectra of the solutions used for single droplet combustion and FSP. The range between 2800 and 4000 cm^{-1} is characteristic of the CH and OH stretching modes. In the spectrum of pure xylene, the peaks observed at 2970, 2924 and 2872 cm^{-1} are assigned to symmetric and asymmetric stretching modes of the methyl groups, while the signature around 3025 cm^{-1} is due to the CH stretching in the aromatic ring. The strongest peaks are found in the finger-print region, originating from CH deformation, CC stretching and bending as well as breathing modes of the aromatic ring [26]. The spectrum of pure Tin 2-ethylhexanoate exhibits signals at 2959, 2937, 2878, and 2866 cm^{-1}. They are analogously assigned to asymmetric/symmetric stretching vibrations of the CH groups of Sn-hexanoate. In addition, the presence of a peak at 1710 cm^{-1} is due to C = O stretching vibrations of the free carboxylic acid group while the 1538 cm^{-1} band is a characteristic signal of COO–Sn–OOC. The spectra of the precursor-solvent mixtures show systematic changes with increasing precursor concentration. In order to identify solvation effects, the difference spectra were analyzed (Fig. 2c). They show several S-shaped signatures at 690, 742, 768, and 796 cm^{-1}, which coincide with the strong signatures in the xylene spectrum. Interestingly, the mixture spectrum with the lowest concentration of the Sn-precursor shows a small deviation from the trend of the other spectra around 1710 cm^{-1}. The difference spectrum exhibits a minor S-shaped signature. This may be interpreted in terms of a molecular interaction between the carboxyl oxygen of the precursor and the π-electrons of the aromatic ring in the solvent. Similar effects between polar groups and aromatic rings were observed before, e.g. in mixtures between acetone and an imidazolium ionic liquid [27] and between alcohol and a graphite surface [28].

From the FTIR analysis of the precursor solutions we conclude that the Tin 2-EHA precursor is chemically inert with Xylene before the solution is fed into the droplet generator or FSP nozzle. In other words, the chemical decomposition of the precursor and the formation of tin oxide exclusively takes place during the actual process (that is single droplet combustion or the spray flame).

3.2 Single droplet combustion

Figure 3a shows merged image sequences of the single burning droplets containing 0, 0.05, 0.1, 0.25, 0.5, 0.75 and 1 mol/L Tin 2-EHA/Xylene (left to right). In each merged image sequence, the time intervals between two continuous droplet positions are 1.45, 1.85, 1.475, 1.125, 1.25, 1.4, and 1.075 ms, which corresponds to the high-speed camera captured frame intervals of 58, 74, 59, 45, 50, 56 and 43, respectively. The pure Xylene droplet combusts continuously, while the other six Tin 2-EHA/Xylene droplets experience micro-explosions after a short period of continuous combustion (as marked with a red dashed circle). The corresponding high-speed camera recorded videos are provided in Supporting Information Video S1. It is seen from the videos that, the surface of the Tin 2-EHA/Xylene droplets explodes away and the inner part of the parent droplet forms a new child droplet. The surface of the new child droplet also explode away after a short period of steady combustion. This repeated process makes the droplet micro-explosions continuous. For example, four times droplet micro-explosions were observed during the single droplet combustion of 0.5

mol/L Tin 2-EHA/Xylene (see Fig. S1). Hereby, surface micro-explosion is proposed as a new definition to describe the ejective burning behavior of the droplet outer-layer.

Micro-explosion is induced by the superheating and internal boiling of the high-volatility component trapped in the droplet, whose temperature is controlled by the low-volatility component [29]. According to Rosebrock et al. [16], the mechanisms during the combustion of the Tin 2-EHA/Xylene droplets follow three steps: (1) diffusion-controlled combustion of the high-volatility component (d-square law, i.e., the squared droplet diameter decreases linearly with time), and accumulation of the low-volatility component at droplet surface, (2) thermal decomposition of the low-volatility precursor at droplet surface and subsequent formation of the assumed viscous shell, and (3) surface micro-explosion owing to pressure build-up caused by the heterogeneous vapor nucleation of the high-volatility component beneath the shell. In our study, the assumed “viscous shell”composes of intermediates from liquid-phase thermal decomposition of the precursor, the undecomposed precursor, and xylene, which is considered mostly in liquid-phase and has a high viscosity. The formation of the assumed viscous shell is proposed based on the experimental observation of continuous droplet surface micro-explosions, which is weaker but multiple compared to micro-explosions of slurry droplets. The decomposition of the metal-organic precursor is a key to the formation of the assumed viscous shell and subsequent heterogeneous vapor nucleation during the micro-explosion of precursor/solvent droplets. Intermediates from thermal decomposition of the precursor, together with the undecomposed precursor and part of xylene at the droplet surface, are assumed to take part in the formation of shell, whose inner surface is considered to provide sites for subsequent heterogeneous vapor nucleation. The occurrences of heterogeneous vapor phase nucleation in the near surface area of Tin 2-EHA/Xylene droplets can be supported by our previous work, where the radial locations within the Tin 2-EHA/Xylene droplets showing the occurrences of heterogeneous and homogeneous vapor phase nucleation have been simulated [22]. The comparison with the experimental explosion times demonstrate that the limits of heterogeneous vapor phase nucleation instead of homogeneous vapor phase nucleation in the near surface area of Tin 2-EHA/Xylene droplets can be reached [22].

Micro-explosion can also be observed during miscible and emulsified multicomponent droplet combustion. During miscible multicomponent droplet combustion, micro-explosion is highly depended of the volatility differences and liquid-phase diffusion resistance of the multiple components [30, 31]. Only using proper compositions and components, droplet explosions can occur [32, 33]. It is different with the continuous surface explosions taking place during single droplet combustion of precursor solutions, where the occurrence of micro-explosion is independent on the precursor concentration. During emulsified multicomponent droplet combustion, the occurrence of micro-explosions depends on both compositions and components [34], and the time scale needed for micro-explosions is less than that of miscible multi-component droplet [35]. Furthermore, the degree of the disruptive burning behavior is either too strong (Explosion: for example the whole droplet breaks up into small droplets quickly) or too weak (Puffing, for example, water vapor is blown out from the droplet surface during water-in-oil emulsion droplet combustion) [36]. It is different with the three-step micro-explosion mechanism during the combustion of the Tin 2-EHA/Xylene droplets.

The sketch of the mechanism of the droplet surface micro-explosion, and related experimental images of 0.5 mol/L Tin 2-EHA/Xylene droplet are shown in Fig. 3b and c, respectively. After ignition (marked with red dashed circle at 0 ms in Fig. 3c), the high-volatility Xylene first evaporates to the flame, leaving low-volatile Tin 2-EHA concentrates at the droplet surface (preferential evaporation). As more Tin 2-EHA accumulates at the droplet surface, less Xylene can diffuse from the droplet into the flame. The evaporation-cooling rate reduces and thus the droplet starts to heat up. Moreover, the flame front subsequently moves closer to the droplet surface, increasing the heat transfer from flame front to droplet *via* conduction and radiation. As a result, the surface temperature rises. The simulated temperature and composition profiles of Tin 2-EHA/Xylene droplets can be found in our previous work [22]. Due to high temperature, the Tin 2-EHA at the droplet surface decomposes into solid, liquid and gaseous intermediates. The gas, solid and liquid intermediates together with the undecomposed low-volatility component form the assumed viscous shell. Due to the inhibition effect of the shell on evaporation, the flame will continue to move closer to the droplet surface (Flame shrinkage, as seen in Fig. 3a) and heat the surface. In other words, the controlling of the droplet surface temperature is changed from the high-volatility component (mainly Xylene) to the low-volatility component (mainly Tin 2-EHA and its decomposed intermediates), because of the composition changes at the droplet surface [37]. Consequently, the high-volatility component (mixture containing mainly xylene) beneath the shell will be overheated to induce heterogeneous vapor nucleation, leading to pressure build-up beneath the shell until the occurrence of surface micro-explosion. The outer layer of the droplet is ejected away (marked with red dashed circle at 6.025 and 6.050 ms) because it is the location of the shell and the heterogeneous nucleation. The inner part of the droplet near the core will form a new droplet (marked with red dashed circle at 6.575 ms) due to surface tension, and continue to burn and explode. These steps are in accordance with the normalized TGA and DTA analysis (see Fig. 4). The data show that pure Xylene vaporizes completely up to its boiling point (139 °C). Contrary, pure Tin 2-EHA precursor starts to decompose in the temperature range from 160 to 475 °C, with the largest mass loss rate at about 320 °C. The 0.5 and 1 mol/L Tin 2-EHA/Xylene solutions lie midway, i.e. they show a large mass loss up to 165 °C and then exhibit decomposition. These observations are in line with the pure components, designating the initial Xylene vaporization and subsequent thermal decomposition of Tin 2-EHA precursor. At 165 °C, the weight losses of 0.5 and 1 mol/L Tin 2-EHA/Xylene solutions are 76.5% and 56.7%, respectively. These numbers are almost exactly the same as the mass fractions of xylene in the prepared solutions (76.6% and 56.6% xylene in the 0.5 and 1 mol/L Tin 2-EHA/Xylene solutions, respectively). Due to the slow heating rate, Xylene will totally evaporate first and explosions are prevented. The remaining weight of the 0.5 and 1 mol/L Tin 2-EHA/Xylene solutions are 6.8% and 13.1%, respectively. These values reasonably agree with the calculated SnO_2 mass fractions of 8.1% and 15.0% based on the compositions of the initial solutions.

Tin 2-EHA is a metalorganic precursor with typical carboxylate structure, where one Sn ion bonds to two 2-ethylhexanoates. During metal-organic decomposition (MOD) techniques, metal-organic precursors with carboxylate structures can pyrolyze cleanly to metal oxides [38, 39]. TG studies of metal 2-ethylhexanoates normally shows a multistep process, which

can be characterized using distinct transition temperatures [39, 40]. Based on the TG results shown in Fig. 4 and Table S1, the liquid-phase thermal decomposition process of Tin 2-EHA/Xylene is described using the scheme in Fig. 5. Xylene evaporates from 30 to 165 °C. The removal of the first 2-ethylhexanoate group occurs from 165 to 310 °C. From 310 to 475 °C the second 2-ethylhexanoate group is removed, forming amorphous SnO_2 particles. The proposed thermal decomposition process is based on the good fit between the normalized remaining weight of 0.5 and 1 mol/L Tin 2-EHA/Xylene with theory calculation (Table S2 and Fig. S2). The theory calculation assumes that the component is $Sn(C_8H_{15}O_2)_2$, $Sn(C_8H_{15}O_2)_1$, and SnO_2 at 165, 310 and 475 °C, respectively.

Figure 6 shows the evolutions of the normalized diameter and the burning constant of the droplets as obtained from the high-speed camera imaging. The droplet diameter changes are normalized based on the averaged value from ten highly reproducible burning droplets, and the maximum of the standard deviation is less than 1.9 μm (Fig. S3). The burning constant decreases with increasing precursor concentration, because of the large heat of vaporization of the precursor. The heat of vaporization at the boiling point of Xylene is 341 kJ/kg, and the heat of vaporization at the boiling point of Tin 2-EHA is considered as that of 2-ethylhexanoic acid (528 kJ/kg) [41]. The evolutions of the normalized diameters of the Tin 2-EHA/Xylene droplet mostly follow the classical D-square law. Taking 0.75 mol/L Tin 2-EHA/Xylene droplet as an example (red curve in Fig. 6(a)), the normalized diameter initially decreases linearly, but levels out for a short period of time at around 0.08 μs/μm^2, and then decreases linearly again. This staged burning phenomenon can be attributed to the droplet heating [32, 42], where the low volatility precursor accumulates at the droplet surface and requires heat for its thermal decomposition and evaporation. As a result, the droplet burning constant will slowly drop for a short period (see the inflection points of the burning constant in Fig. 6(b)), and flame contraction or shrinkage occurs [22, 37]. Taking the volume changes during the droplet combustion into account, the normalized volumes of the droplet at the moment of the first surface micro-explosion and at the moment of the inflection point increase with the precursor concentration (Fig. S4). This indicates that, with increase of the precursor concentration, the occurrences of the shell formation and subsequent surface micro-explosions are accelerated. The occurrence of the inflection point (staged burning and flame contraction) comes earlier as the increase of the low volatility precursor, which is consistent with the previous investigation. Shaw et al. [42] observed the staged burning and flame contraction for methanol/dodecanol droplets, and attributed it to the sudden droplet heating that occurs as a result of a build-up of the low volatility component.

3.3 Nanoparticles synthesis via FSP

Figure 7(a) shows the photographs of the spray flames in the FSP experiments of Tin 2-EHA/Xylene solutions. The flame color changes from white to yellow with increasing Sn molar concentration. As a first step, the FSP-synthesized SnO_2 nanoparticles are characterized *via* BET specific surface area (SSA) and the BET particle diameter (average equivalent primary particle size), as shown in Fig. 7(b). The BET diameters of these nanoparticles obtained from Tin 2-EHA/Xylene solutions increase from 5.2, 6.0, 7.9, 9.2, 10.0, to 11.1 nm (uncertainty: < 0.3 nm) with Sn molar concentration increase from 0.05, 0.1, 0.25, 0.5, 0.75 to 1 mol/L, respectively.

The particle crystallite size increases with increasing Sn molar concentration, which is demonstrated by the decreasing width of the XRD peaks from 0.05 to 1 M Tin 2-EHA/Xylene solutions in Fig. 8. The refinements of the XRD patterns were performed using BRASS program [43–45]. The crystallite size of these nanoparticles increase from 3, 3.6, 4.9, 5.9, 6.8, to 7.5 nm for FSP synthesis using Tin 2-EHA/Xylene solutions with Sn molar concentration increase from 0.05, 0.1, 0.25, 0.5, 0.75 to 1 mol/L, respectively.

During gas-to-particle conversion in the FSP powder synthesis, the gas-phase precursor flows and reacts at high temperature. The product vapor starts to form particles when experiencing lower temperatures and further growth by condensation and /or coagulation [46]. The high-temperature particle residence time and the interplay of surface growth, coagulation and sintering determine the size, composite and morphology of flame-made particles [47]. The high-temperature particle residence time (few milliseconds) can be considered the same for these sprays in terms of almost the same flame heights (Fig. 7). The high precursor concentration solution provides more nucleation seeds in the spray flame, leading to higher coagulation rates and large dense agglomerates of primary particles and consequent large particles [48]. Similar results are reported for the flame synthesized Titania and Zirconia nanoparticles [48, 49].

3.4 TEM measurements and nanoparticle comparison

The representative TEM images, particle size distributions, and high-resolution TEM (HRTEM) images of SnO_2 particles obtained from FSP and single droplet combustion are shown in Figs. 9–11, S5, S6, and S7. The particle size distributions are determined using the DigitalMicrograph software (Gatan, Inc) to analyze around 500 nanoparticles for each sample. The HRTEM images reveal high crystallinity of these particles. The flame-made particles are highly agglomerated, containing large (> 20 nm), middle (10–20 nm) and small (< 10 nm) particles. However, droplet-made particles show two different types: the large rectangular nanoparticles (e.g., Fig. 9, middle) with wide size distribution, and small almost spherical nanoparticles (e.g., Fig. 9, right) with narrow size distribution. Both types of particles are considered to be produced *via* the gas-to-particle conversion, because of their nanoscale size and homogeneous morphology. During single droplet combustion of one precursor solution, these two types of nanoparticles were collected at the same copper grid. However, their deposition locations at the same copper grid are separable, indicating other probable particle formation pathways or different locations and/or periods.

With the increase of the precursor concentration, the flame-made particle size increases and the size distribution becomes wider, as proved by the representative TEM images and particle size distribution plots (see Figs. 9, and –11), respectively. The particle size increases with precursor concentration, which is consistent with the BET and XRD measurements. Similar conclusion is extracted for the droplet-made large particles, showing a similar size distribution as the flame-made particles. The size and size distribution of the droplet-made small particles exhibit slight fluctuations with varying precursor concentrations, indicating the formation of ultrafine homogenous nanoparticles.

Figure 12 shows the size comparison of particles obtained from FSP and single droplet combustion (SD) using TEM, BET and XRD measurements. The XRD and BET results

show that both the crystallite size and the average equivalent primary particle size increase with the precursor concentration, respectively. The crystallite size measured by XRD is smaller than the average equivalent primary particle size measured by BET, which is mainly caused by agglomerated and aggregated particles making the BET measured SSA smaller than the real SSA. The mean particle size of the small ultrafine particles obtained from single droplet combustion (SD-small) agree reasonably in the crystallite size, indicating most of these small spherical particles are single crystallites. The characteristics of particles synthesized from FSP and single droplet combustion experiments are summarized in Table 1.

Although their direct experimental observations are still lacking, droplet explosions are likely to take place in the spray flame as well. This is also indicated by previous investigations [49, 50]. Tani et al. [49] investigated the morphology of Zinc oxide/silica particles made by spray combustion, and suggested fragments of the droplets in the spray flame on the basis of the large size difference between particle and the dispersed droplet. Jang et al. [50] indicated that the disintegration of large precursor droplets into small droplets would occur because of the high temperature gradient between the droplets and the high flame temperature during FSP. Therefore, assuming droplet micro-explosions occurring in FSP, these two types of SnO_2 nanoparticles observed during single droplet combustion maybe possibly be obtained in the spray flame as well. Thus, the flame-made particles can be considered as the mixture of these two types of particles, where the mixture is caused by the experimental conditions in FSP including interaction of droplets, high flame temperature, high thermal gradient, and turbulence. This assumption is further supported by the similar size and crystallinity between flame-made and droplet-made SnO_2 particles. Furthermore, assuming the two types of drople-made particles have the same amount (Quantity ratio: 1:1), the mean particle diameter of the mixture (red solid circle) fits well with the particle diameter of flame-made particles (black hollow circle), as shown in Fig. 12.

3.5 Proposed mechanism of particle formation

During the single droplet combustion of Tin 2-EHA/Xylene solutions, the precursor-solvent droplets start to burn steadily after ignition until the occurrence of the first surface micro-explosion. The occurrences of droplet surface micro-explosion are multiple and no residuals are observed at the end of droplet combustion. These findings are supported by the high-speed camera recorded videos provided in Supporting information Video S1. Therefore, the nanoparticles can only be formed during (1) the period from ignition to first surface micro-explosion, (2) the instant process of droplet surface micro-explosion, and (3) the periods between two consecutive surface micro-explosions. It is assumed that the large rectangular SnO_2 particles originate from the droplet surface micro-explosions, where the fuel is secondarily atomized into small ejected fragments (see Fig. 3c at 6.050 and 6.075 ms, as well as high-speed camera recorded videos provided in Supporting information Video S1.). The precursor (from the inner of the shell) and the intermediates (from the liquid-phase thermal decomposition of the precursor around the shell) were carried by the ejected fragments to the flame. During this instant process, the ejected fragments are first violently spread out to form a widely distributed droplet cluster, which can mix well with the surrounding oxygen. Then the droplet cluster starts to burn from the outside to the inside.

This supports the complete combustion of the ejected fuels, evidenced by the large and white flame luminosity in Fig. 3c at 6.425 and 6.450 ms (more information can be found in high-speed camera recorded videos provided in Supporting information Video S1.). During droplet surface micro-explosions, the fast evaporation of the liquid fuel into the gas phase results in an accelerated reaction due to atomization. The extra heat release from the flame, and the subsequent fast sintering caused by the contact with the cold co-flowing gas promote homogeneous nanoparticle formation *via* gas-to-particle conversion, which has been proved using low volatile nitrate precursors [14]. Increasing the precursor concentration reduces the time to explosion (Fig. S6), and increases the precursor concentration in the ejected fragments. Consequently, the particle size becomes larger, which has been shown by the TEM results. The small and almost spherical SnO_2 particles are considered to be obtained during the period from ignition to the first micro-explosion as well as during the periods between two consecutive surface micro-explosions; accurately, the period from the inflection point to the micro-explosion occurrence, as shown in Fig. S8. During this period, the precursor accumulates at the droplet surface, absorbs more heat from the flame, and probably decomposes to reach another quasi-steady state, where the low-volatility precursor dictates the surface temperature [22]. The precursor and/or its thermally decomposed intermediates take part in the assumed viscous shell formation. At the same time, it can transfer slowly from droplet surface to the flame due to the increased droplet surface temperature. This kind of mass transfer is slower compared to droplet surface micro-explosions. The low density of the precursor and/or its thermally decomposed intermediates in the gas phase reduces the initial particle number density, supporting the synthesis of ultrafine nanoparticles. Increasing the precursor concentration prolongs the period from the inflection point to the micro-explosion occurrence (Fig. S8). As a result, more small ultrafine SnO_2 particles are found in the droplet combustion of high concentration precursor solutions. This is supported by the TEM measurements, where it is much easier to find small ultrafine SnO_2 particles synthesized from droplet combustion of high concentration precursor solutions.

In order to explain the transfer of Sn atoms from liquid phase into gas phase, two nanoparticle formation paths during single droplet combustion are proposed: (1) steady combustion and (2) droplet surface micro-explosion (see Fig. 13). During steady combustion, the Tin 2-EHA and its intermediates (from thermal liquid-phase decomposition) exposed at the droplet surface could absorb heat from flame, evaporate into vapors, and diffuse to the flame front. At the flame front, the fuel vapors undergo gas-phase thermal decomposition, and Sn atoms in Tin 2-EHA and its intermediates are finally oxidized into SnO_2 vapors. SnO_2 vapors start nucleating in the colder flame regions due to supersaturation, followed by particle growth (*via* coagulation and sintering), aggregation and agglomeration. During droplet surface micro-explosion, due to surface tension, the ejected fragments form a cluster of small droplets, which contain mainly Tin 2-EHA and its decomposed intermediates, *i.e.*, a high concentration of Sn atoms. This promotes the formation of high concentration supersaturation of SnO_2 vapor and subsequent more nucleation seeds in the flame. As a result, larger nanoparticle are formed. Different with the formation of amorphous SnO_2 particles during TG, crystalline nanoparticle are formed

during single droplet combustion because of the amorphous-to-crystalline phase transition at a higher temperature created by the flame.

4 Summary and conclusions

Flame spray pyrolysis has successfully been employed to synthesize and design nanoparticles. However, many of the underlying processes in the liquid-vapor-flame-particle process chain are still not fully understood [23]. Further research is necessary to develop a detailed knowledge and further advance the application potential of FSP. Therefore, we conducted a careful experimental investigation to determine the precursor decomposition and particle formation during single droplet combustion, in order to provide fundamental information for FSP process.

SnO_2 nanoparticles were synthesized *via* flame spray pyrolysis as well as single droplet combustion using the same metal-organic solutions. The stability and vaporization behavior of these solutions were analysed using FTIR spectroscopy and TGA, respectively. The FTIR spectra and TGA profiles clarified that the chemical decomposition of the precursor and the formation of tin oxide exclusively take place during the actual process and not during the preparation of the initial solution. The thermal decomposition of the metal-organic precursor and the subsequent shell formation is the cause for the surface micro-explosions during single droplet combustion. The time to explosion reduces with the increase of the precursor concentration. This is explained by the faster accumulation of low-volatile compounds at the droplet surface.

The nanoparticles obtained from FSP and single droplet combustion exhibit similar size and crystallization, while the particle sizes increase with the increased metal-precursor concentration. TEM images of particles from single droplet combustion reveal two types of nanoparticles with different size distributions and morphologies. Two nanoparticle formation paths during single droplet combustion are proposed. The large SnO_2 particles are considered to be obtained from the droplet surface micro-explosions, where the secondary atomization of the fuel and subsequent fast heat release and reaction facilitate the homogenous particle formation. The small SnO_2 particles are assumed to synthesize during the period from the inflection point to the micro-explosion occurrence (steady combustion), where the accumulated precursor and its thermally decomposed intermediates at the droplet surface could transfer to the flame.

It is pointed out that due to resolution limitations of the currently available optical techniques such as rainbow refractometry, interferometric particle imaging, and high-speed digital camera imaging, more detailed and accurate information is difficult to obtain *in-situ*. This includes the structure, density, thickness of the shell, and the early particle formation during the steady droplet combustion and droplet surface micro-explosions. Therefore, the explanations of the particle formation during single droplet combustion are derived from the set of our current experimental results. Nano-scale and molecular-scale approaches, for example, X-Ray free electron laser based method, are proposed for future investigations in order to further unravel the mechanisms of the particle generation and surface micro-explosions. This, however, is the subject of a separate study. Moreover, both differences and

Europe PMC Funders Author Manuscripts

similarities exist between single droplet combustion and the group droplet combustion in FSP. Thus, more detailed and deeper investigations are needed to identify them.

Supplementary Material

Refer to Web version on PubMed Central for supplementary material.

Acknowledgements

HL, JK, and LM thank the Deutsche Forschungsgemeinschaft (DFG) for funding this research within the priority program SPP 1980 SPRAYSYN under grants of MA 3333/14-1 and KI1396/6-1. SP and LM would also like to thank European Research Council (ERC) for funding the work under grant agreement “ReSuNiCo 786487”. The authors would like to thank Horst Woyczechowski from Leibniz Institute for Materials Engineering IWT for providing technical supports for the droplet-on-demand generators, Tina Kühn from Institute of Advanced Ceramics, University of Bremen for providing helps with TGA measurements, and Dr. Michael Wendschuh from Central Laboratory for Crystallography and Applied Materials, University of Bremen for providing helps with XRD measurements. The authors also thank Lizoel Buss from Leibniz Institute for Materials Engineering IWT for providing the raw data of particle residence time and original particle number concentration during FSP.

References

[1]. Teoh WY, Amal R, Mädler L. Flame spray pyrolysis: an enabling technology for nanoparticles design and fabrication. Nanoscale. 2010; 2:1324–1347. [PubMed: 20820719]

[2]. Li S, Ren Y, Biswas P, Tse SD. Flame aerosol synthesis of nanostructured materials and functional devices: processing, modeling, and diagnostics. Prog Energy Combust Sci. 2016; 55:1–59.

[3]. Mädler L, Kammler H, Mueller R, Pratsinis SE. Controlled synthesis of nanostructured particles by flame spray pyrolysis. J Aerosol Sci. 2002; 33:369–389.

[4]. Buss L, Meierhofer F, Bianchi Neto P, França Meier H, Fritsching U, Noriler D. Impact of co-flow on the spray flame behaviour applied to nanoparticle synthesis. Can J Chem Eng. 2019; 97:604–615.

[5]. Strobel R, Pratsinis SE. Effect of solvent composition on oxide morphology during flame spray pyrolysis of metal nitrates. Phys Chem Chem Phys. 2011; 13:9246–9252. [PubMed: 21468418]

[6]. Harra J, Kujanpää S, Haapanen J, Juuti P, Mäkelä JM, Hyvärinen L, Honkanen M. Aerosol analysis of residual and nanoparticle fractions from spray pyrolysis of poorly volatile precursors. AIChE J. 2017; 63:881–892.

[7]. Grossmann HK, Grieb T, Meierhofer F, Hodapp MJ, Noriler D, Grohn A, Meier HF, Fritsching U, Wegner K, Mädler L. Nanoscale mixing during double-flame spray synthesis of heterostructured nanoparticles. J Nanopart Res. 2015; 17:174.

[8]. Strobel R, Pratsinis SE. Flame aerosol synthesis of smart nanostructured materials. J Mater Chem. 2007; 17:4743–4756.

[9]. Okuyama K, Lenggoro IW. Preparation of nanoparticles via spray route. Chem Eng Sci. 2003; 58:537–547.

[10]. Messing GL, Zhang SC, Jayanthi GV. Ceramic powder synthesis by spray pyrolysis. J Am Ceram Soc. 1993; 76:2707–2726.

[11]. Lenggoro IW, Itoh Y, Iida N, Okuyama K. Control of size and morphology in NiO particles prepared by a low-pressure spray pyrolysis. Mater Res Bull. 2003; 38:1819–1827.

[12]. Arutanti O, Arif AF, Balgis R, Ogi T, Okuyama K, Iskandar F. Tailored synthesis of macroporous Pt/WO_3 photocatalyst with nanoaggregates via flame assisted spray pyrolysis. AIChE J. 2016; 62:3864–3873.

[13]. Abram C, Mezhericher M, Beyrau F, Stone HA, Ju Y. Flame synthesis of nanophosphors using sub-micron aerosols. Proc Combust Inst. 2019; 37:1231–1239.

[14]. Rosebrock CD, Wriedt T, Mädler L, Wegner K. The role of microexplosions in flame spray synthesis for homogeneous nanopowders from low-cost metal precursors. AIChE J. 2016; 62:381–391.

Europe PMC Funders Author Manuscripts

[15]. Meierhofer F, Li H, Gockeln M, Kun R, Grieb T, Rosenauer A, Fritsching U, Kiefer J, Birkenstock J, Mädler L, Pokhrel S. Screening precursor-solvent combinations for $Li_4Ti_5O_{12}$ energy storage material using flame spray pyrolysis. ACS Appl Mater Interfaces. 2017; 9:37760–37777. [PubMed: 28960057]

[16]. Rosebrock CD, Riefler N, Wriedt T, Mädler L, Stephen DT. Disruptive burning of precursor/solvent droplets in flame-spray synthesis of nanoparticles. AIChE J. 2013; 59:4553–4566.

[17]. Li H, Rosebrock C, Riefler N, Wriedt T, Mädler L. Experimental investigation on microexplosion of single isolated burning droplets containing titanium tetraisopropoxide for nanoparticle production. Proc Combust Inst. 2017; 36:1011–1018.

[18]. Skenderovic I, Kotalczyk G, Kruis FE. Dual population balance Monte Carlo simulation of particle synthesis by flame spray pyrolysis. Processes. 2018; 6:253.

[19]. Sahm T, Mädler L, Gurlo A, Barsan N, Pratsinis SE, Weimar U. Flame spray synthesis of tin dioxide nanoparticles for gas sensing, Sens. Actuat B – Chem. 2004; 98:148–153.

[20]. Van den Broek J, Abegg S, Pratsinis SE, Güntner A. Highly selective detection of methanol over ethanol by a handheld gas sensor. Nat Commun. 2019; 10:1–8. [PubMed: 30602773]

[21]. Kemmler JA, Pokhrel S, Madler L, Weimar U, Barsan N. Flame spray pyrolysis for sensing at the nanoscale. Nanotechnology. 2013; 24

[22]. Li H, Rosebrock CD, Wu Y, Wriedt T, Mädler L. Single droplet combustion of precursor/solvent solutions for nanoparticle production: optical diagnostics on single isolated burning droplets with micro-explosions. Proc Combust Inst. 2019; 37:1203–1211.

[23]. Schulz C, Dreier T, Fikri M, Wiggers H. Gas-phase synthesis of functional nanomaterials: challenges to kinetics, diagnostics, and process development. Proc Combust Inst. 2019; 37:83–108.

[24]. Ulmke H, Wriedt T, Bauckhage K. Piezoelectric droplet generator for the calibration of particle sizing instruments. Chem Eng Technol. 2001; 24:265–268.

[25]. Riefler N, Wriedt T. Generation of monodisperse micron-sized droplets using free adjustable signals. Part Part Syst Char. 2008; 25:176–182.

[26]. Lindenmaier R, Scharko NK, Tonkyn RG, Nguyen KT, Williams SD, Johnson TJ. Improved assignments of the vibrational fundamental modes of ortho-, meta-, and paraxylene using gas- and liquid-phase infrared and Raman spectra combined with ab initio calculations: quantitative gas-phase infrared spectra for detection. J Mol Struct. 2017; 1149:332–351.

[27]. Kiefer J, Molina MM, Noack K. The peculiar nature of molecular interactions between an imidazolium ionic liquid and acetone. ChemPhysChem. 2012; 13:1213–1220. [PubMed: 22344818]

[28]. Kiefer J, Toni F, Wirth K-E. Influence of carbon-coated iron nanoparticles on the Raman spectrum of liquid ethanol. J Raman Spectrosc. 2015; 46:1124–1128.

[29]. Botero M, Huang Y, Zhu D, Molina A, Law CK. Synergistic combustion of droplets of ethanol, diesel and biodiesel mixtures. Fuel. 2012; 94:342–347.

[30]. Rao DCK, Karmakar S, Som S. Puffing and micro-explosion behavior in combustion of butanol/Jet A-1 and acetone-butanol-ethanol (ABE)/Jet A-1 fuel droplets. Combust Sci Technol. 2017; 189:1796–1812.

[31]. Law CK. Combustion physics. 2006:595–622.

[32]. Wang C, Liu X, Law CK. Combustion and microexplosion of freely falling multicomponent droplets. Combust Flame. 1984; 56:175–197.

[33]. Lasheras J, Fernandez-Pello A, Dryer F. On the disruptive burning of free droplets of alcohol/n-paraffin solutions and emulsions. Symp (Int.) Combust. 1980:293–305.

[34]. Avulapati MM, Ganippa LC, Xia J, Megaritis A. Puffing and micro-explosion of diesel-biodiesel-ethanol blends. Fuel. 2016; 166:59–66.

[35]. Lasheas J, Yap L, Dryer F. Effect of the ambient pressure on the explosive burning of emulsified and multicomponent fuel droplets. Symp (Int.) Combust. 1985; 20:1761–1772.

[36]. Watanabe H, Matsushita Y, Aoki H, Miura T. Numerical simulation of emulsified fuel spray combustion with puffing and micro-explosion. Combust Flame. 2010; 157:839–852.

[37]. Hoxie A, Schoo R, Braden J. Microexplosive combustion behavior of blended soybean oil and butanol droplets. Fuel. 2014; 120:22–29.

[38]. Rousseau B, Phok S, Ortega L, Guibadj N, Wegelius T, Morlens S, Odier P, Weiss F, Eikmeyer J. CeO_2 epitaxial films by spray mod. J Eur Ceram Soc. 2005; 25:2185–2189.

[39]. Mishra S, Daniele S, Hubert-Pfalzgraf LG. Metal 2-ethylhexanoates and related compounds as useful precursors in materials science. Chem Soc Rev. 2007; 36:1697–1844.

[40]. Xue S, Ousi-Benomar W, Lessard R. α-Fe_2O_3 thin films prepared by metalorganic deposition (MOD) from Fe(III) 2-ethylhexanoate. Thin Solid Films. 1994; 250:194–201.

[41]. Lide, DR. CRC handbook of chemistry and physics. 88th ed. CRC Press; 2007.

[42]. Shaw BD, Dwyer HA, Wei JB. Studies on combustion of single and double streams of methanol and methanol/dodecanol droplets. Combust Sci Technol. 2002; 174:29–50.

[43]. Birkenstock, J, Fischer, R, Messner, T. BRASS: The Bremen Rietveld Analysis and Structure Suite. University of Bremen; Bremen: 2010. Ver. 2.2 Beta

[44]. Pokhrel S, Birkenstock J, Schowalter M, Rosenauer A, Mädler L. Growth of ultrafine single crystalline WO_3 nanoparticles using flame spray pyrolysis. Cryst Growth Des. 2010; 10:632–639.

[45]. Pokhrel S, Birkenstock J, Dianat A, Zimmermann J, Schowalter M, Rosenauer A, Ciacchi LC, Mädler L. In situ high temperature X-ray diffraction, transmission electron microscopy and theoretical modeling for the formation of WO_3 crystallites. CrystEngComm. 2015; 17:6985–6998.

[46]. Pratsinis SE, Vemury S. Particle formation in gases: a review. Powder Technol. 1996; 88:267–273.

[47]. Kelesidis GA, Goudeli E, Pratsinis SE. Flame synthesis of functional nanostructured materials and devices: surface growth and aggregation. Proc Combust Inst. 2017; 36:29–50.

[48]. Pratsinis SE, Zhu W, Vemury S. The role of gas mixing in flame synthesis of titania powders. Powder Technol. 1996; 86:87–93.

[49]. Tani T, Takatori K, Pratsinis SE. Evolution of the morphology of zinc oxide/silica particles made by spray combustion. J Am Ceram Soc. 2004; 87:365–370.

[50]. Jang H, Seong C, Suh Y, Kim H, Lee C. Synthesis of lithium-cobalt oxide nanoparticles by flame spray pyrolysis. Aerosol Sci Technol. 2004; 38:1027–1032.

Europe PMC Funders Author Manuscripts

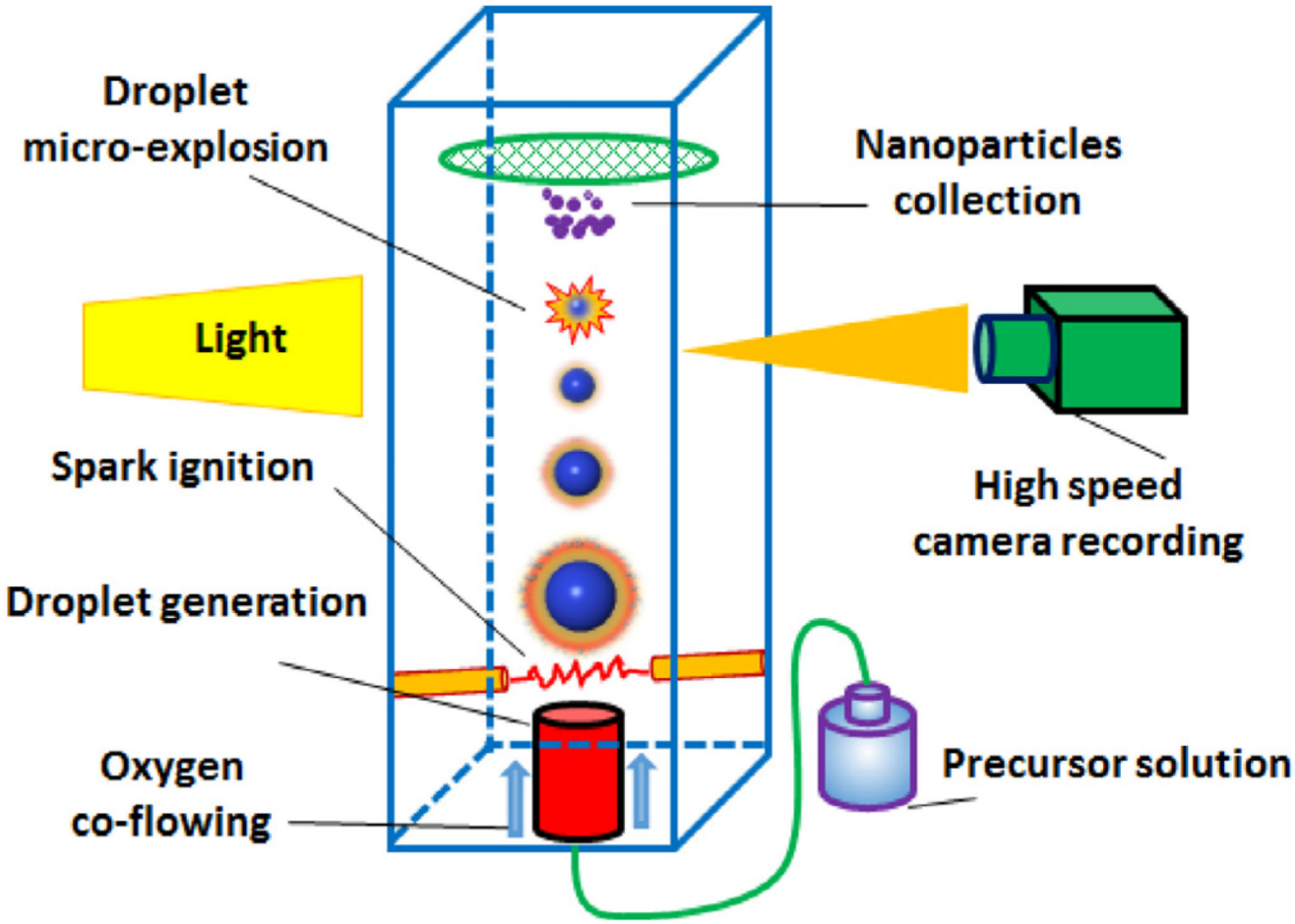

Fig. 1.
Sketch of experimental setup for single isolated droplet combustion.

Europe PMC Funders Author Manuscripts

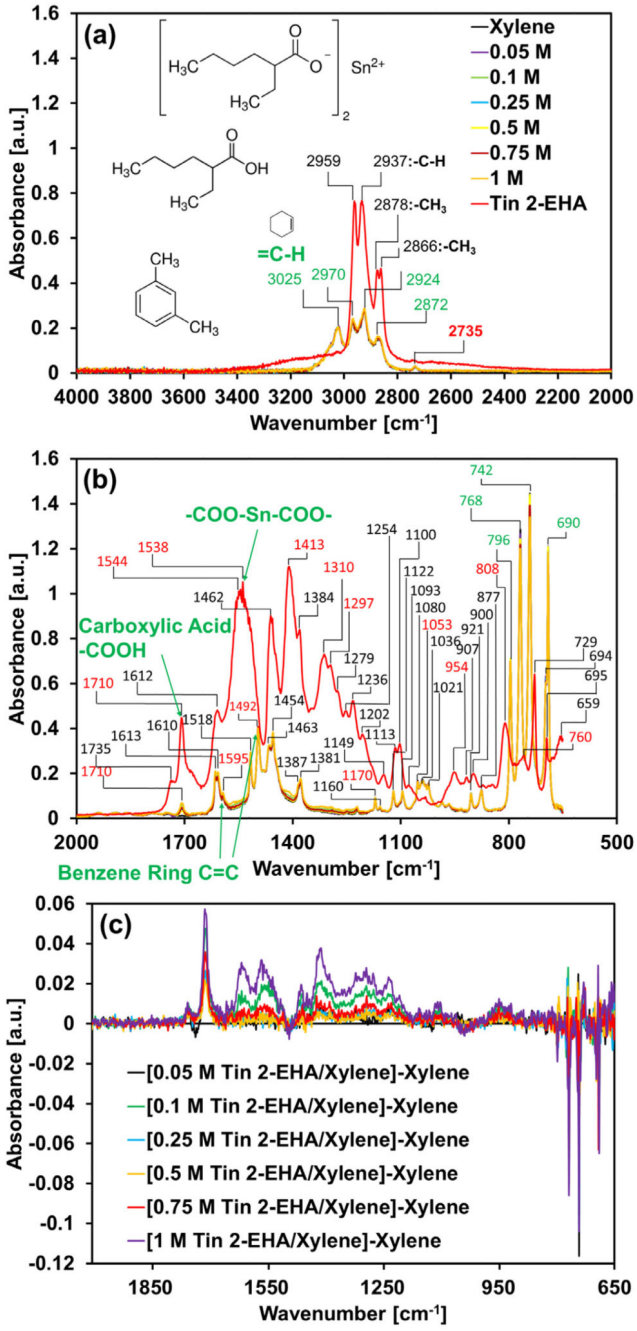

Fig. 2.

The FTIR spectra analysis of the solutions in single droplet combustion and FSP: (a) in the range of 2000–4000 cm^{-1}, (b) in the range of 650–2000 cm^{-1} and (c) the difference spectra between the precursor-solvent mixtures and Xylene. (For interpretation of the references to color in this figure legend, the reader is referred to the web version of this article.)

Europe PMC Funders Author Manuscripts

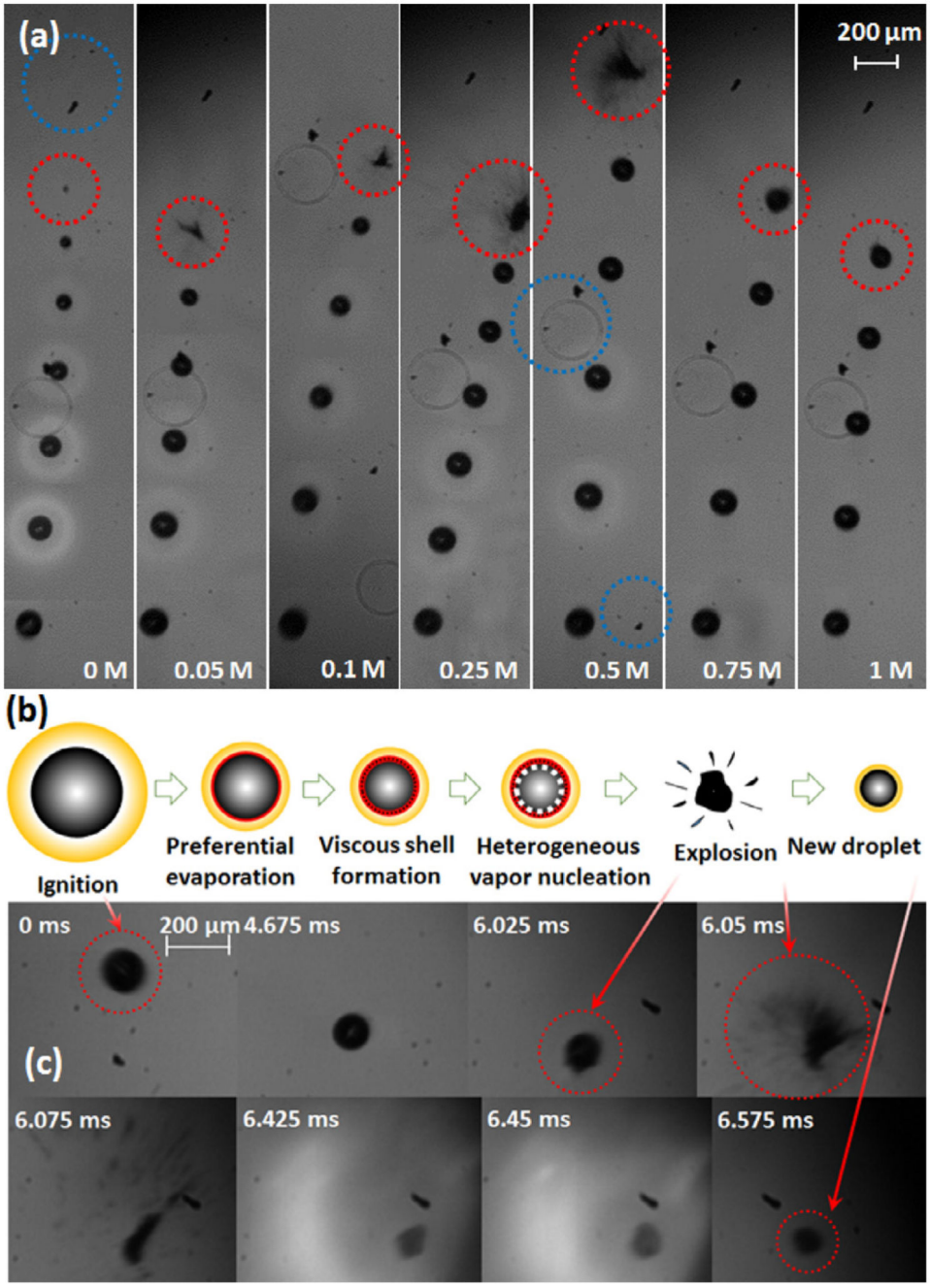

Fig. 3.

(a) Merged image sequences of isolated burning droplets: from left to right, the molar concentration of Tin 2-EHA/Xylene droplets increase from 0, 0.05, 0.1, 0.25, 0.5, 0.75 to 1 mol/L. From bottom to top the droplets move in the upwards direction in the experiment. The initial droplet image is obtained from the high-speed camera recorded frame at the moment of ignition. Contaminations on the lens of the high-speed camera are marked with blue dashed circles. The corresponding high-speed camera recorded videos are provided in Supporting Information Video S1. (b) Micro-explosion mechanism of burning precursor/

solvent droplet, and (c) the recorded images of the combustion process of 0.5 mol/L Tin 2-EHA/Xylene droplet via shadowgraphy (bottom). The time interval is measured from the moment of ignition. (For interpretation of the references to color in this figure legend, the reader is referred to the web version of this article.)

Europe PMC Funders Author Manuscripts

Europe PMC Funders Author Manuscripts

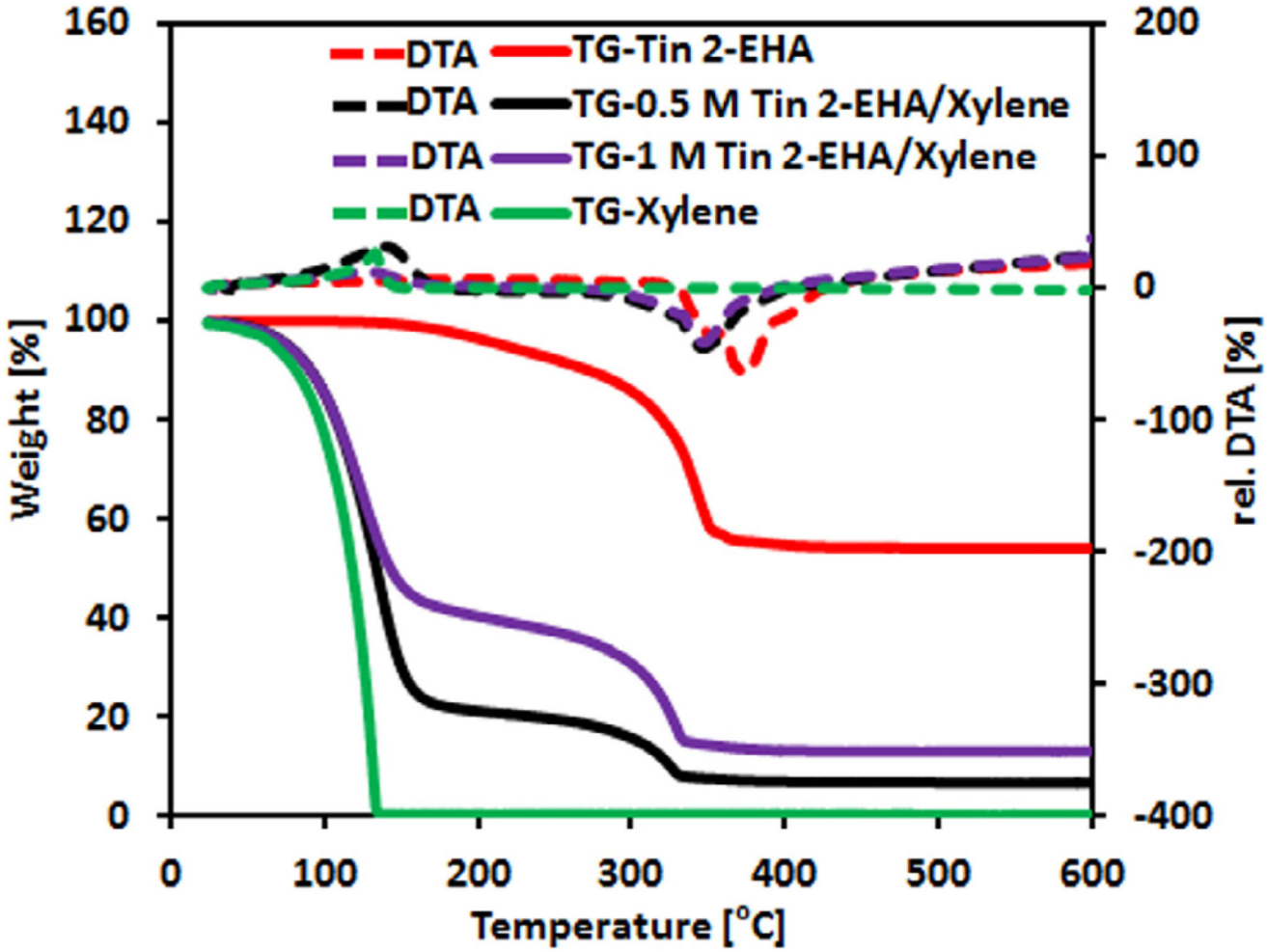

Fig. 4.

Normalized TGA weight loss (solid line, left axis) and DTA signal (square dotted line, right axis) for Tin(II) 2-ethylhexanoate (red), 0.5 mol/L Tin 2-EHA/Xylene (black), 1 mol/L Tin 2-EHA/Xylene (purple) and Xylene (green). The measurements were conducted at a temperature increase rate of 7.5 °C/min. (For interpretation of the references to color in this figure legend, the reader is referred to the web version of this article.)

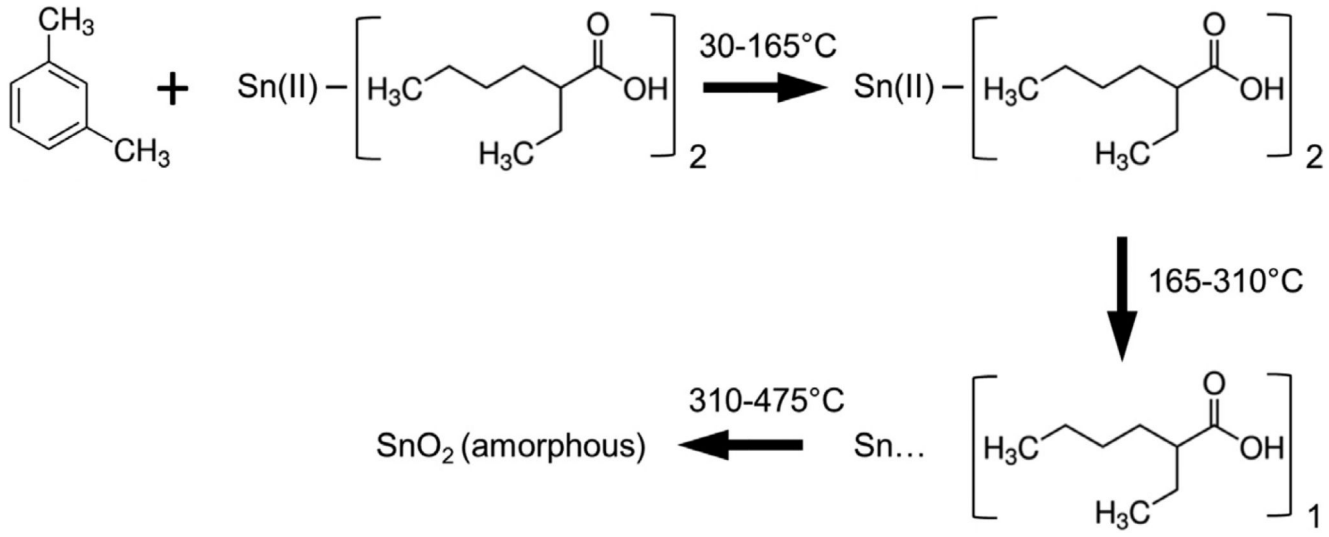

Fig. 5.

The scheme showing the three-stage liquid-phase thermal decomposition process of Tin 2-EHA/Xylene in the temperature range from 30 to 475 °C.

Europe PMC Funders Author Manuscripts

Europe PMC Funders Author Manuscripts

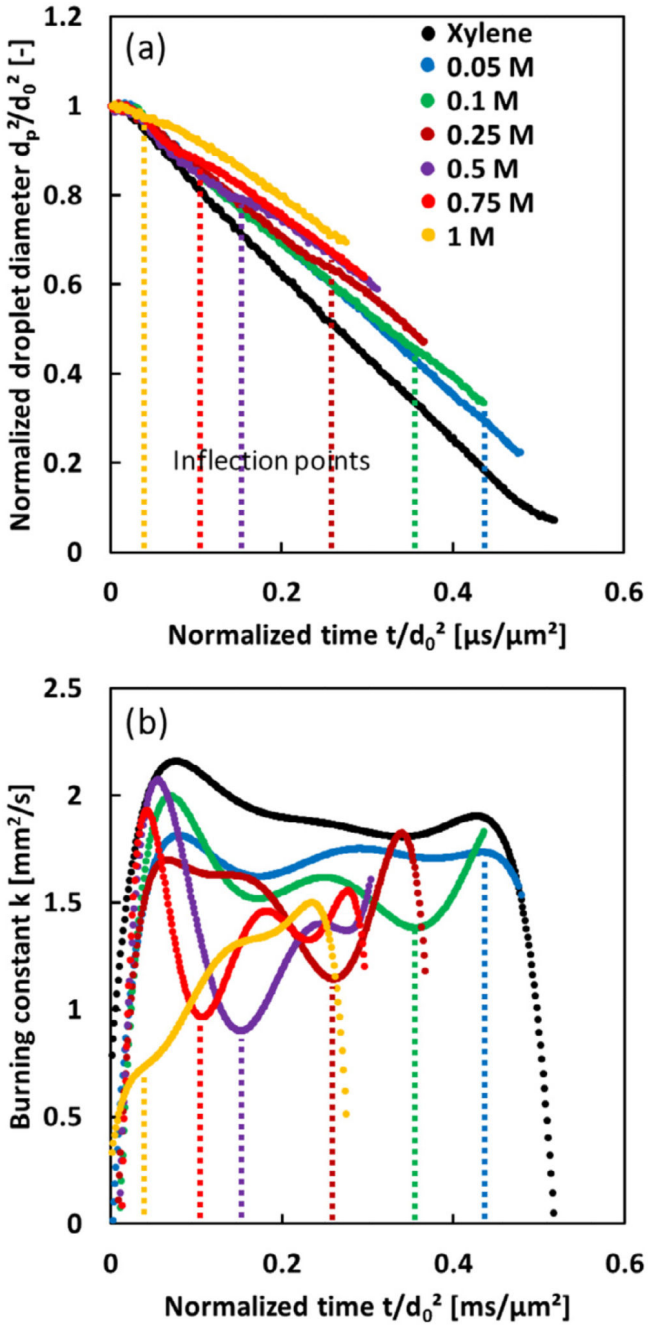

Fig. 6.

(a) Normalized droplet diameter changes for Tin 2-EHA/Xylene droplets. The ignition of the droplet corresponds to a normalized time equal to zero with a droplet diameter to d_0. (b) Burning constant. The dashed lines mark the time for inflection points of the burning constant. (For interpretation of the references to color in this figure, the reader is referred to the web version of this article.)

Europe PMC Funders Author Manuscripts

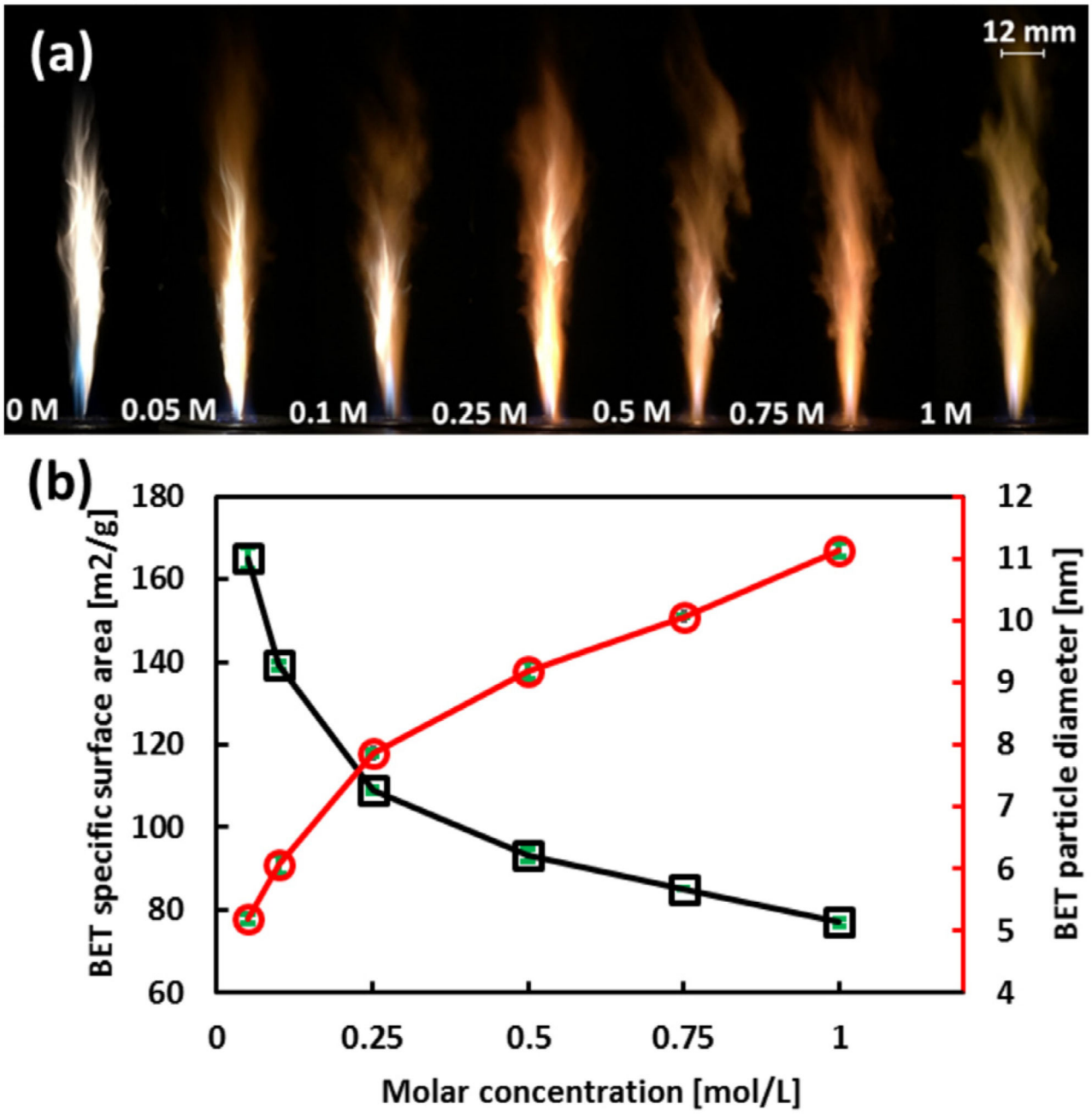

Fig. 7.

(a) Photographs of the spray flames in FSP experiments of Tin 2-EHA/Xylene solutions with molar concentrations of 0, 0.05, 0.1, 0.25, 0.5, 0.75 and 1 mol/L. The lengths of these flames are in the range from 100 to 120 mm. These photographs were taken with reduced light intensity in the background. (b) The BET surface area (black square, left axis) and BET particle diameter (red circle, right axis) for SnO_2 nanoparticles obtained from FSP. (For interpretation of the references to color in this figure legend, the reader is referred to the web version of this article.)

Europe PMC Funders Author Manuscripts

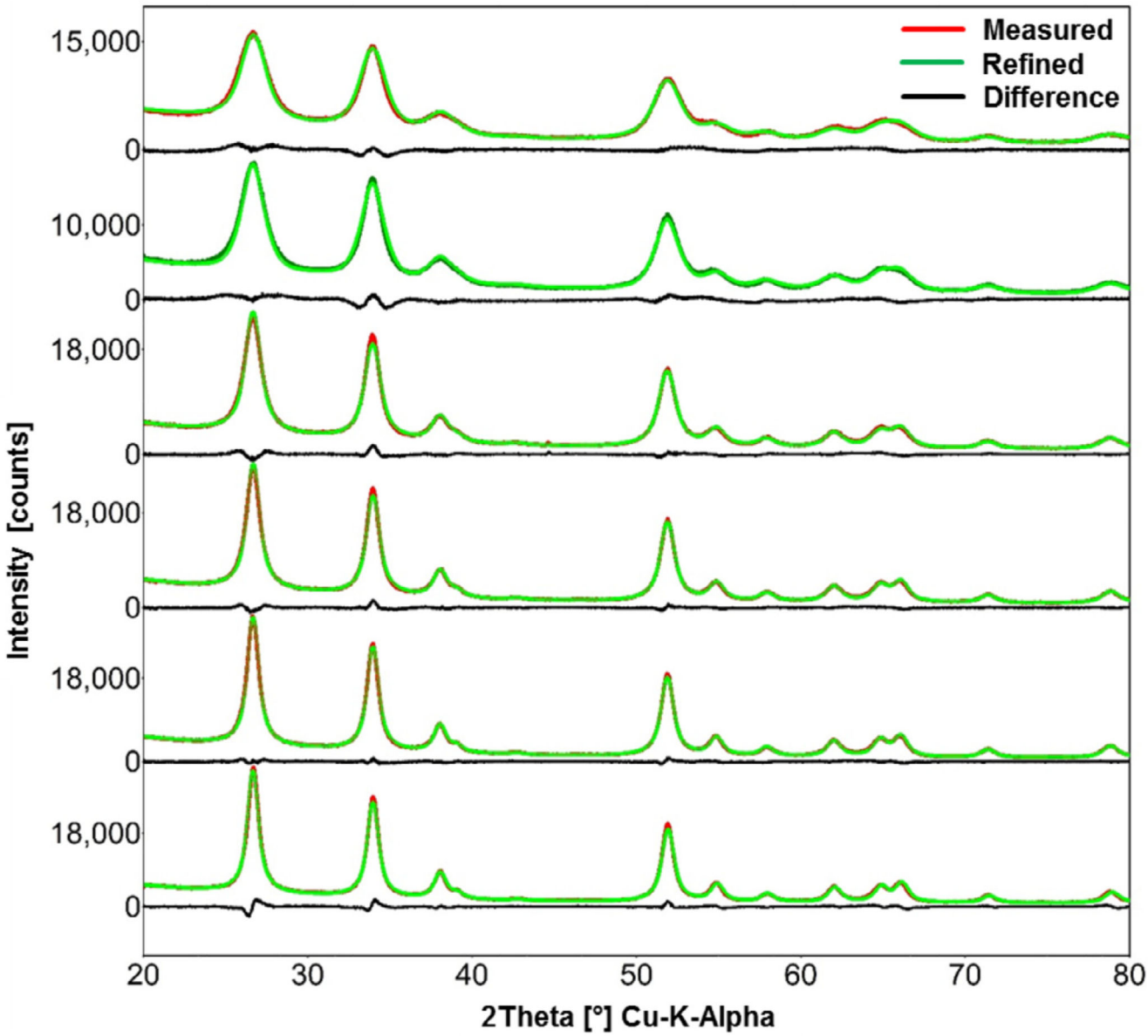

Fig. 8.

XRD patterns (red curve) and Rietveld refinements (green curve) of SnO_2 particles obtained from FSP using 0.05, 0.1, 0.25, 0.5, 0.75 and 1 mol/L Tin 2-EHA/Xylene solutions. The difference between the measured and refined data is represented by the black curves. The widths of the peaks decrease with the increased precursor concentration, revealing the increase of the crystallite size of these particles. (For interpretation of the references to color in this figure legend, the reader is referred to the web version of this article.)

Europe PMC Funders Author Manuscripts

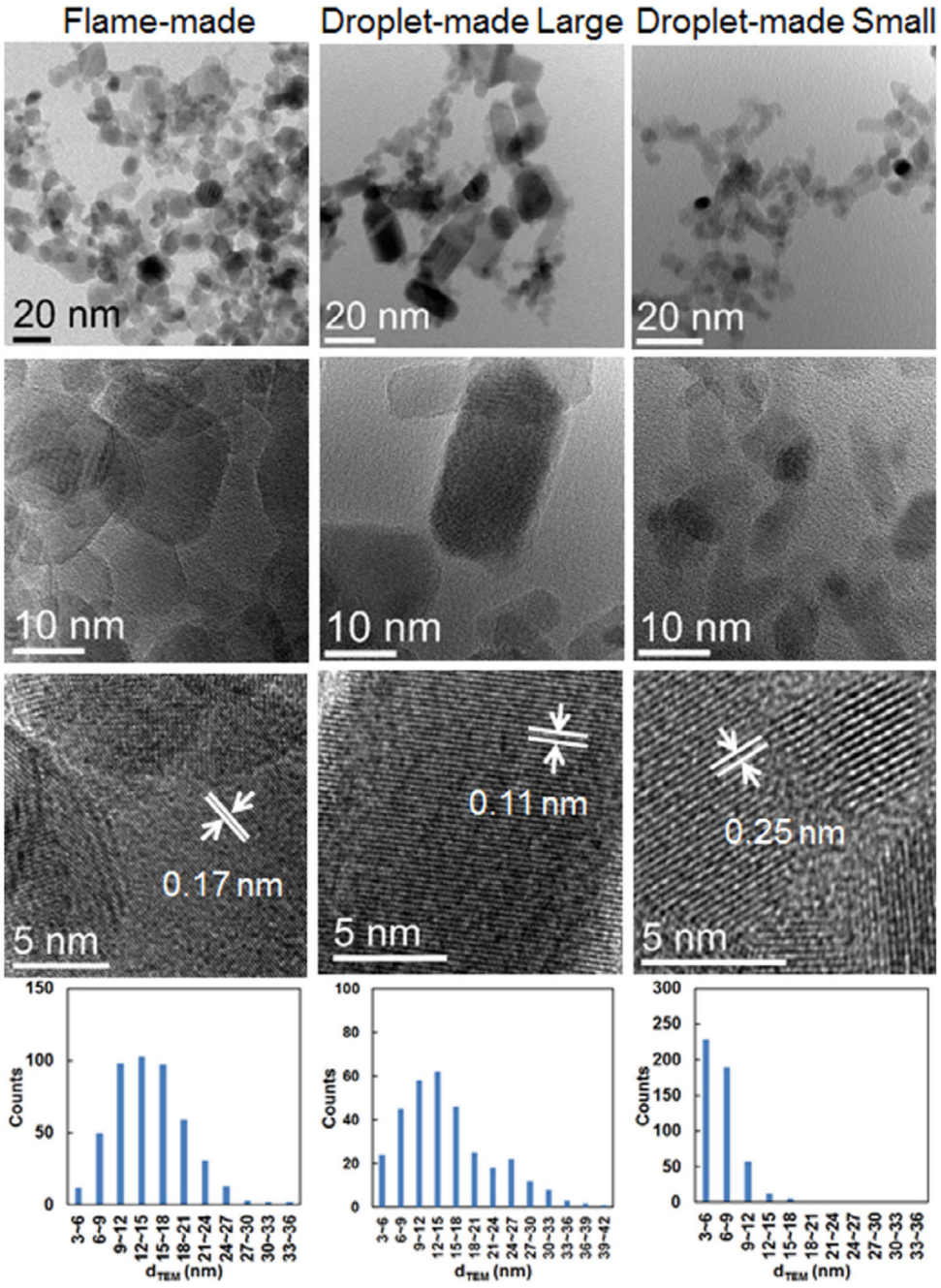

Fig. 9.

TEM images, high-resolution TEM (HRTEM) images, and size distributions of SnO_2 nanoparticles obtained from FSP and single droplet combustion for 1 mol/L Tin 2-EHA/ Xylene. Droplet-made particles reveals two different types: the large rectangular nanoparticles (middle) with wide size distributions, and small almost spherical nanoparticles (right) with narrow size distributions. In HRTEM images, the differences of lattice fringe spacing are due to the different plane orientations.

Europe PMC Funders Author Manuscripts

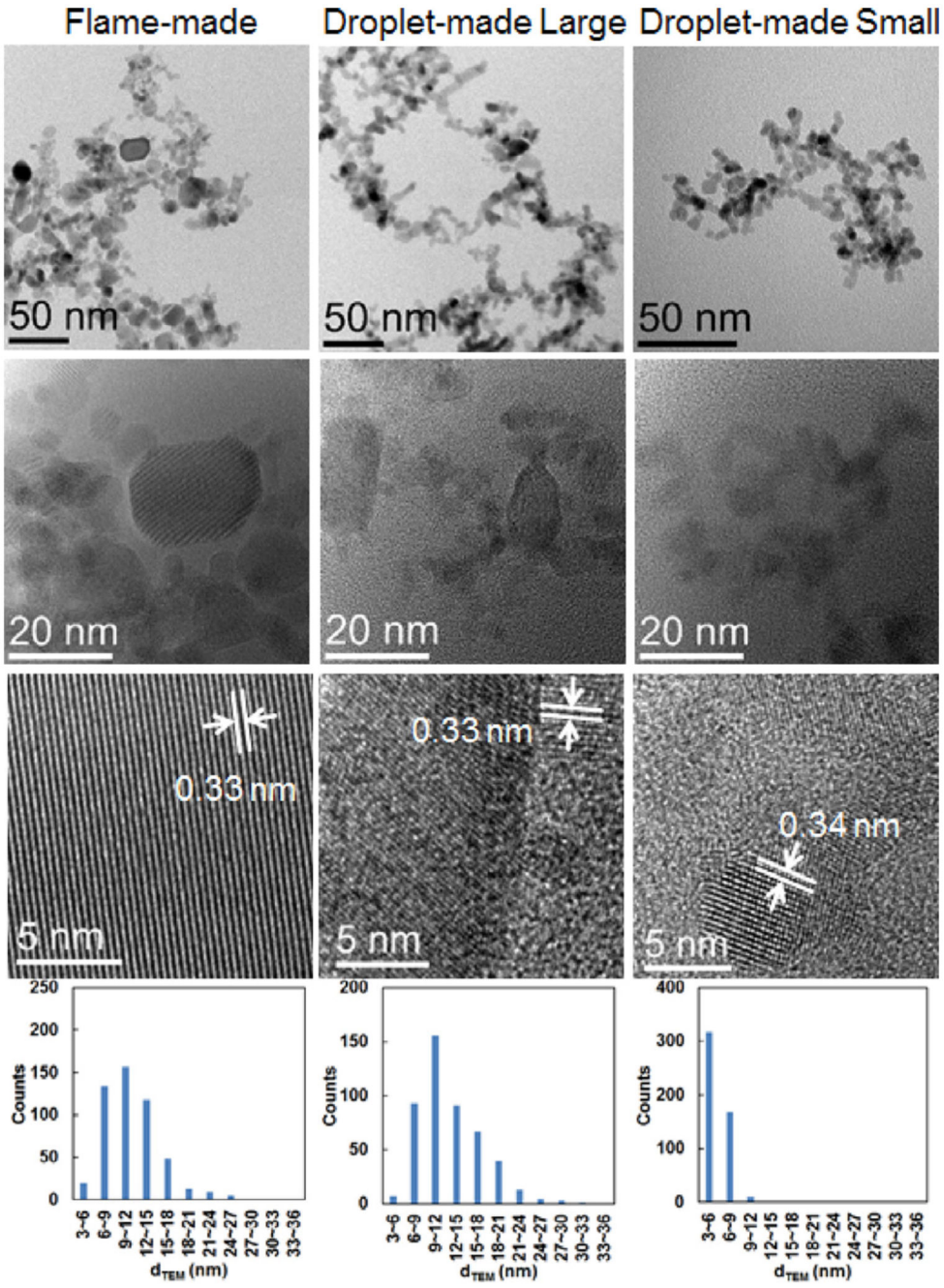

Fig. 10.

TEM images, high-resolution TEM (HRTEM) images, and size distributions of SnO_2 nanoparticles obtained from FSP and single droplet combustion for 0.5 mol/L Tin 2-EHA/ Xylene.

Europe PMC Funders Author Manuscripts

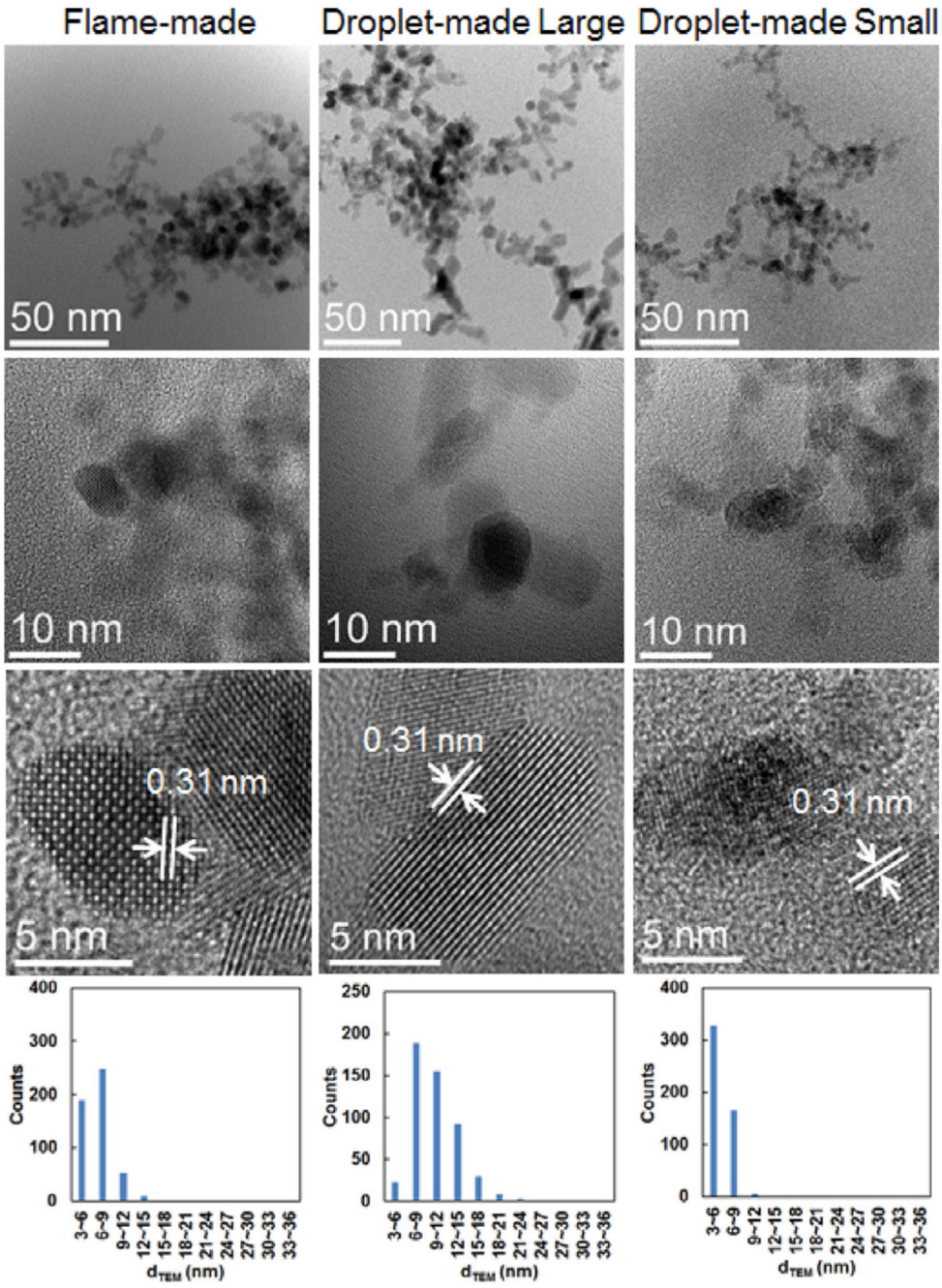

Fig. 11.

TEM images, high-resolution TEM (HRTEM) images, and size distributions of SnO_2 nanoparticles obtained from FSP and single droplet combustion for 0.1 mol/L Tin 2-EHA/ Xylene.

Europe PMC Funders Author Manuscripts

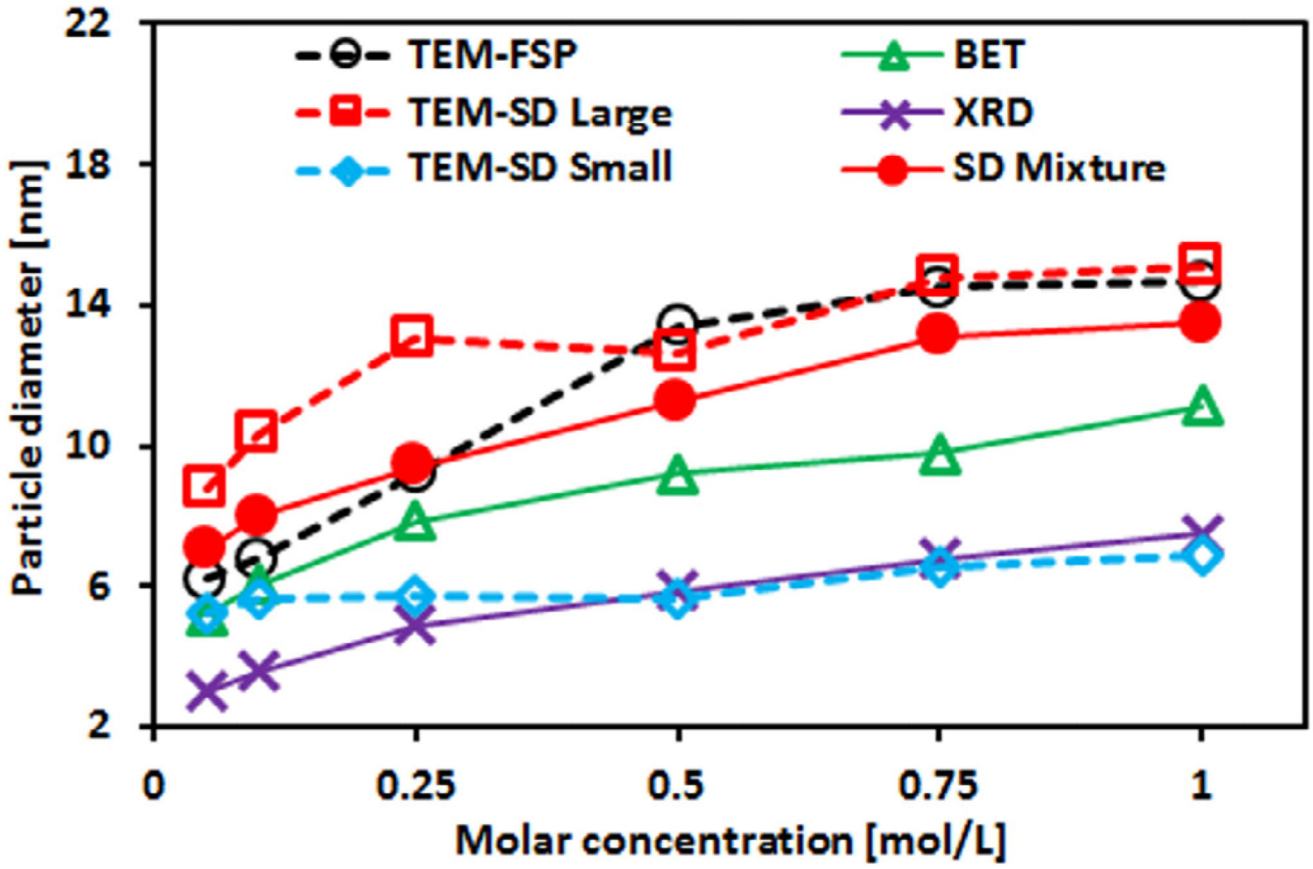

Fig. 12.

Size comparison of particles obtained from FSP and single droplet combustion (SD) using TEM, BET and XRD measurements. Black hollow circle, red hollow square, and blue hollow diamond represent the particle diameters measured using TEM for flame-made particles, and droplet-made small and large particles, respectively. Green hollow triangle and purple cross is the flame-made particle diameters measured using BET and XRD, respectively. Red solid circle represent the mean particle diameter of the two types SnO_2 particles synthesized via single droplet combustion, assuming both have the same amount. (For interpretation of the references to color in this figure legend, the reader is referred to the web version of this article.)

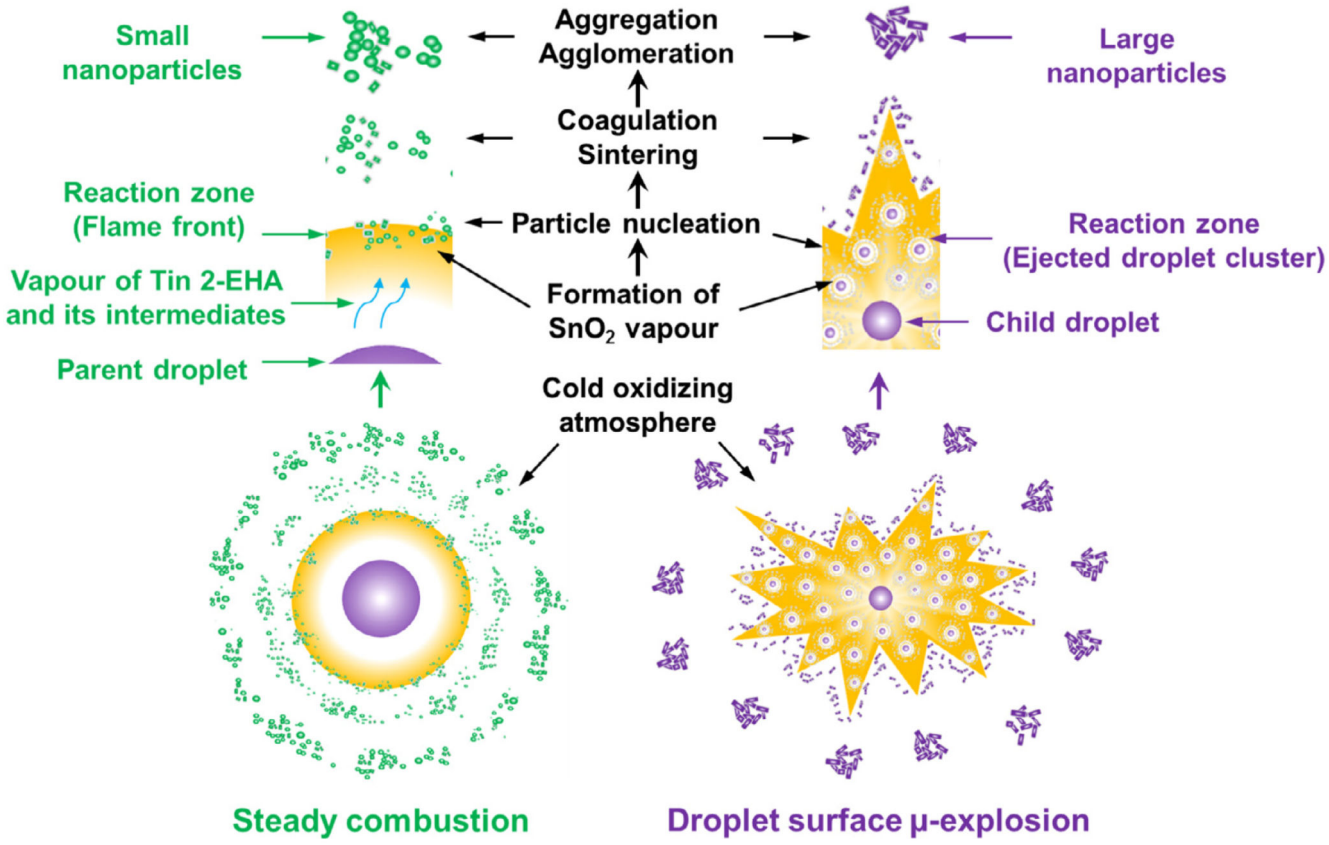

Fig. 13.

Schematic illustration of the two nanoparticle formation paths during single droplet combustion of Tin 2-EHA/Xylene: steady combustion (left) and droplet surface μ-explosion (right).

Europe PMC Funders Author Manuscripts

Europe PMC Funders Author Manuscripts

Table 1

The characteristics of particles synthesized from FSP and single droplet combustion experiments.

	Particles synthesized via FSP (flame-made particles)	Particles synthesized via single droplet combustion (droplet-made particles)	
Abbreviation	Flame-made	Droplet-made large	Droplet-made small
Size scale	Nano-scale	Nano-scale	Nano-scale
Morphology	Highly agglomerated, cuboid and spherical	Cuboid	Almost spherical
Size distribution	Wide	Wide	Narrow
Crystallization	Multiple crystallite	Multiple crystallite	Single crystallite